

# SageAttention2 Technical Report: Accurate 4 Bit Attention for Plug-and-play Inference Acceleration

Jintao Zhang\*, Haofeng Huang\*, Pengle Zhang, Jia Wei, Jun Zhu, Jianfei Chen

*Tsinghua University*

## Abstract

Although quantization for linear layers has been widely used, its application to accelerate the attention process remains limited. SageAttention utilizes 8-bit matrix multiplication, 16-bit matrix multiplication with 16-bit accumulator, and precision-enhancing methods, implementing an accurate and 2x speedup kernel compared to FlashAttention2. To further enhance the efficiency of attention computation while maintaining precision, we propose **SageAttention2**, which utilizes significantly faster 4-bit matrix multiplication (Matmul) alongside additional precision-enhancing techniques. First, we propose to quantize matrixes ( $Q, K$ ) to INT4 in a warp-level granularity and quantize matrixes ( $\tilde{P}, V$ ) to FP8. Second, we propose a method to smooth  $Q$  and  $V$ , enhancing the accuracy of attention with INT4  $QK$  and FP8  $PV$ . Third, we analyze the quantization accuracy across timesteps and layers, then propose an adaptive quantization method to ensure the end-to-end metrics over various models. The operations per second (OPS) of **SageAttention2** surpass FlashAttention2 and xformers by about **3x** and **5x** on RTX4090, respectively. Comprehensive experiments confirm that our approach incurs negligible end-to-end metrics loss across diverse models—including those for large language processing, image generation, and video generation. The codes are available at <https://github.com/thu-ml/SageAttention>.

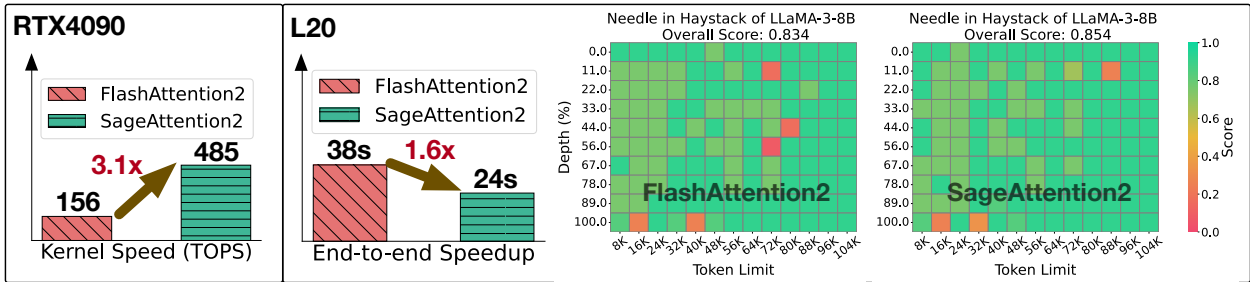


Figure 1: The left figure shows the kernel speedup on RTX4090 GPU. The right figure shows the end-to-end inference speedup of generating the first token and performance metrics for the needle-in-a-haystack task (gkamradt, 2023) with a sequence length of 100K on Llama3.1 on L20 GPU.

\* Equal Contribution.

# 1 Introduction

Due to the quadratic complexity of attention, efficient implementation becomes increasingly crucial as sequences lengthen in real-world applications (Jiang et al., 2024). Several strategies have been developed to mitigate computational demands of attention —such as (1) *Linear attention* methods (Wang et al., 2020; Choromanski et al., 2020; Yu et al., 2022; Katharopoulos et al., 2020) that reduce complexity to  $O(N)$  and (2) *Sparse attention* methods (Liu et al., 2021; Chu et al., 2021; Li et al.; Xiao et al., 2023b, 2024; Chen et al., 2023; Jiang et al., 2024; Venkataramanan et al., 2023; Gao et al., 2024; Fu et al., 2024) that selectively process parts of the context — these methods are only suitable for a limited range of models and tasks. Widely used attention methods optimize attention by exploiting hardware capacities to enhance the computation speed, such as FlashAttention (Dao et al., 2022), FlashAttention2 (Dao, 2023), FlashAttention3 (Shah et al., 2024), xformers (Lefaudeux et al., 2022), and SageAttention (Zhang et al., 2024). Those works do not omit the computation of attention over parts of the context and achieve impressive speed and precision performance across various models and tasks.

For the two matrix multiplication (Matmul) operations in attention:  $QK^\top$  and  $PV$ , SageAttention accelerates them by quantizing the  $QK^\top$  to INT8 and uses FP16 Matmul with FP16 accumulators for  $PV$ . Moreover, to keep the accuracy of attention, SageAttention proposes smoothing  $K$  by eliminating its channel-wise outliers. SageAttention achieves  $2 \times$  and  $2.7 \times$  speedup than FlashAttention2 and xformers and is the first quantized attention that incurs negligible end-to-end metrics loss across language, image, and video generation models. However, SageAttention has two weaknesses. **(W1)** INT8 Matmul achieves only half the speed of INT4. **(W2)** FP16 Matmul with FP16 accumulators is only compatible with RTX4090 and RTX3090 GPUs. To leverage the faster INT4 tensor cores for  $QK^\top$  and using a method that can generally accelerate  $PV$ , we propose **SageAttention2**, which quantizes  $Q, K$  to INT4 and  $P, V$  to FP8.

**Challenges.** Quantizing  $Q, K$  to INT4 and  $P, V$  to FP8 presents significant challenges. For example, when only per-tensor quantizing  $Q, K$  to INT4, the text-to-video model CogvideoX will generate a completely blurry video (See Figure 2), and Llama2 only achieves a random-guessing-level accuracy of 25% on MMLU. After investigating deeply, we identified three primary challenges: **(C1)** The numerical range of INT4, which in quantization typically spans from  $-7$  to  $7$  and totals 15 numbers (Lin et al., 2024), leads to significant quantization errors when  $Q$  and  $K$  have some abnormal values. **(C2)** In specific layers and timesteps (for text-to-image/video) of some models, quantizing  $Q$  and  $K$  to INT4 and quantizing  $P$  and  $V$  to FP8 introduces noticeable errors in attention computation. These errors in worst-case layers/timesteps significantly impact the precision of the end-to-end output. **(C3)** We discover that the FP32 accumulator designed for FP8 matrix multiplication in the tensor core (*mma.f32.f8.f8.f32*) is actually FP22, specifically with 1 sign bit, 8 exponent bits, and 13 mantissa bits. This will lead to an accuracy loss of  $PV$ .

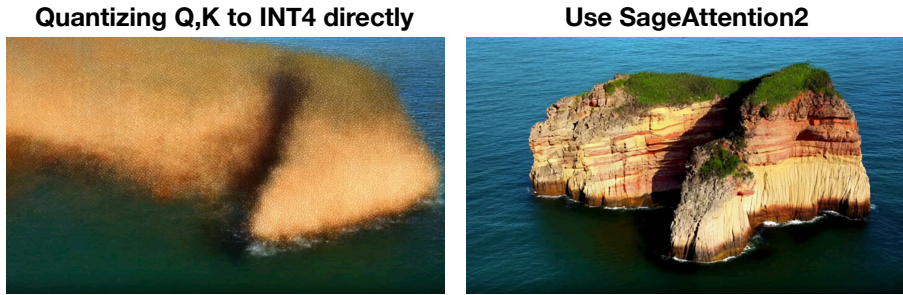


Figure 2: An example of quantizing  $Q, K$  to INT4 from CogvideoX.

**Our approach.** To address these challenges, we detailedly analyze the reasons and propose two methods. First, for the significant channel-wise outliers in matrices  $Q$  and  $K$ , we adopt smoothing  $K$  in SageAttention and propose an effective method to remove these outliers in  $Q$ . Specifically, we propose subtracting the average value of the channel dimension of  $Q$ , referred to as  $\vec{Q}_m$ . Then, we add  $\vec{Q}_m K$  after the  $QK$

Matmul to ensure the correctness of the attention computation. Second, we observe that specific layers and timesteps consistently present quantization challenges across different inputs. To maintain accuracy, we apply an adaptive mix precision method. Specifically, we employ 8-bit (INT8+FP8) attention for these problematic layers and timesteps and 4-bit (INT4+FP8) attention for the others. Third, to mitigate the accuracy loss associated with using the 22-bit accumulator for FP8 Matmul of  $PV$ , we propose a method to smooth  $V$  to enhance the accuracy performance.

**Performance.** Importantly, we offer a high-performance implementation of `SageAttention2` on RTX4090 and L20 GPUs. This implementation achieves a peak performance of **485 TOPS** on the RTX4090, outperforming FlashAttention2 and xformers by approximately 3.1x and 5.4x, respectively. We extensively evaluate the end-to-end metrics of state-of-the-art text, image, and video generation models using `SageAttention2`. Across all models and tasks, `SageAttention2` can be directly adopted in a plug-and-play manner with negligible loss in model performance.

## 2 Preliminary

### 2.1 FlashAttention

The computation of self-attention can be formulated as follows:  $S = QK^\top/\sqrt{d}$ ,  $P = \sigma(S)$ ,  $O = PV$ , where  $\sigma(S)_{ij} = \exp(S_{ij})/\sum_k \exp(S_{ik})$  is the softmax operation. The matrices  $Q$ ,  $K$ , and  $V$  each have dimensions  $N \times d$ , while the matrix  $S$ ,  $P$  are  $N \times N$ . While  $d$  is typically small, e.g., 64 or 128,  $N$  can be thousands if not millions. Therefore, the  $N \times N$  matrices ( $S$ ,  $P$ ) are much larger than ( $Q$ ,  $K$ ,  $V$ ), and a naive implementation suffers from the huge amount of global memory IO for ( $S$ ,  $P$ ) reads/writes. FlashAttention (Dao, 2023) proposes to tile  $Q$ ,  $K$ , and  $V$  from the token dimension into blocks  $\{Q_i\}, \{K_i\}, \{V_i\}$  with block size of  $b_q, b_{kv}, b_{kv}$ , respectively. Then, to avoid the memory IO for ( $S$ ,  $P$ ), it uses online softmax (Milakov & Glimsheim, 2018) to progressively compute each block of  $O$ , i.e.,  $O_i$ :

First, for each block of  $\{K_i\}, \{V_i\}$ , it computes the following equations iteratively:

$$\begin{aligned} S_i^j &= Q_i K_j^\top / \sqrt{d}, \quad (m_i^j, \tilde{P}_i^j) = \tilde{\sigma}(m_i^{j-1}, S_i^j), \quad l_i^j = \exp(m_i^j - m_i^{j-1}) l_i^{j-1} + \text{rowsum}(\tilde{P}_i^j), \\ O_i^j &= \text{diag} \left( \exp(m_i^j - m_i^{j-1}) \right) O_i^{j-1} + \tilde{P}_i^j V_j \end{aligned}$$

Where  $m_i^j$  and  $l_i^j$  are  $b_q \times 1$  vectors, which are initialized to  $-\infty$  and 0 respectively. The  $\tilde{\sigma}()$  is an online softmax operator:  $m_i^j = \max\{m_i^{j-1}, \text{rowmax}(S_i^j)\}$ ,  $\tilde{P}_i^j = \exp(S_i^j - m_i^j)$ .

Finally, the output  $O_i$  can be computed by  $O_i = \text{diag}(l_i^j)^{-1} O_i^j$ .

### 2.2 Quantization

A matrix multiplication  $C = AB$  can be accelerated with quantization as:

$$(\delta_A, \hat{A}) = \psi(A), \quad (\delta_B, \hat{B}) = \psi(B), \quad \hat{C} = \hat{A}\hat{B}, \quad C = \psi_{\delta_A \delta_B}^{-1}(\hat{C}) \quad (1)$$

$\psi$  is a *quantizer* which converts a high-precision (e.g., FP32 or FP16) matrix  $A$  to a low-precision format  $\hat{A}$  (e.g., INT4 or FP8) with a *scale*  $\delta_A$ , and  $\psi^{-1}$  is a *dequantizer* to convert back to high-precision. We should have  $\psi_{\delta_A}^{-1}(\hat{A}) \approx A$ . The actual matrix multiplication  $\hat{A}\hat{B}$  is carried in low-precision. In modern GPUs, low-precision matrix multiplication is usually multiple times faster than higher-precision ones. Many quantizers depend on the numerical format and granularity, e.g., how many elements share a common scale factor. For example, an INT4 *per-tensor quantizer* first computes the scale as the maximum absolute value of the entire tensor, scales the elements to the maximum representable range of INT4  $[-7, +7]$ , and then casts to INT4 with rounding:  $\hat{A} = \lceil A/\delta_A \rceil$ ,  $\delta_A = \max(|A|)/7$ . Likewise, *per-token quantizer* assigns a scale factor for each token of a tensor:  $\hat{A}[i, :] = \lceil A[i, :]/\delta_A[i] \rceil$ ,  $\delta_A[i] = \max(|A[i, :]|)/7$ . Also, *per-channel quantizer* assigns a scale factor for each channel of the tensor, i.e., along the channel dimension:  $A[:, i] = \lceil A[:, i]/\delta_A[i] \rceil$ ,  $\delta_A[i] = \max(|A[:, i]|)/7$ . Dequantization process is a element-wise scaling:  $\psi_{\delta_A \delta_B}^{-1}(\hat{A}\hat{B}) = \hat{A}\hat{B} * \delta_A * \delta_B$ .

### 2.3 SageAttention

Based on the block tiling in FlashAttention2 (Dao, 2023), SageAttention (Zhang et al., 2024) quantize  $Q, K$  to INT8 in a per-block granularity. Moreover, to keep the quantization accuracy, SageAttention proposes to smooth  $K$  first:

$$K = K - \text{mean}(K)$$

$$\hat{Q}_i = \lceil Q_i / \delta_Q \rceil, \quad \delta_Q = \max(|Q_i|) / 127, \quad \hat{K}_j = \lceil K_j / \delta_K \rceil, \quad \delta_K = \max(|K_j|) / 127$$

$$S_{ij} = Q_i K_j^\top * \delta_Q * \delta_K$$

Where  $Q_i, K_j$  are the tiled block in FlashAttention, and  $\text{mean}(K)$  is the average value of the channel dimension of  $K$ . SageAttention keeps  $\tilde{P}V$  as FP16 and uses FP16 Matmul with an FP16 accumulator for  $\tilde{P}V$ . However, FP16 Matmul with an FP16 accumulator only has a speedup effect on RTX4090 and RTX3090 GPUs.

### 3 SageAttention-2

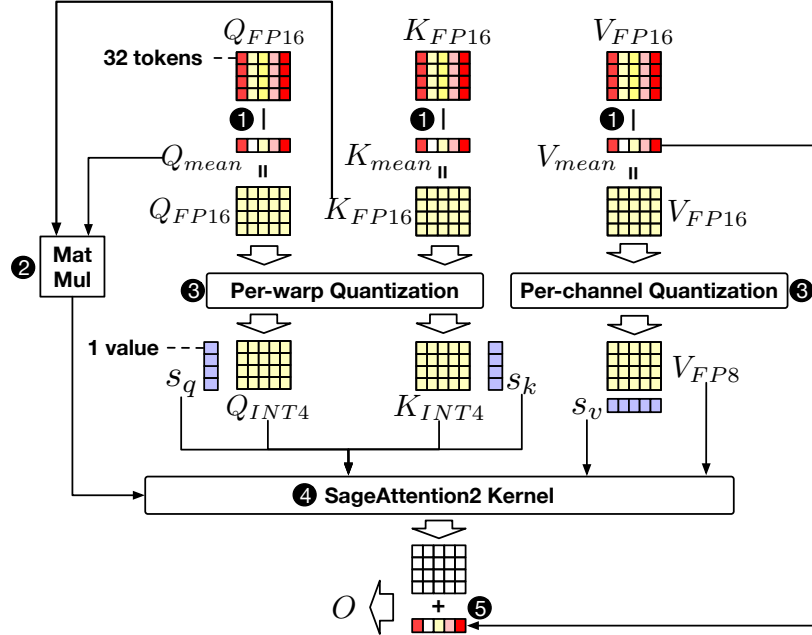


Figure 3: Workflow of SageAttention2. ① Smooth  $Q, K, V$ . ② A GEMV to obtain  $\Delta S$ . ③ Per-warp quantize  $Q, K$  and per-channel quantize  $V$ . ④ Perform the SageAttention2 kernel. ⑤ Correct the output.

### 3.1 Formulation

Based on the introduction of FlashAttention and quantization presented in Section 2, we now describe the quantized attention approach we developed.



$$\text{Quantization: } (\delta_Q, \hat{Q}, \vec{Q}_m) = \phi_Q(Q), \quad (\delta_K, \hat{K}) = \phi_K(K), \quad (\delta_V, \hat{V}, \vec{V}_m) = \phi_V(V)$$

$$\Delta S = \vec{Q}_m \hat{K}^\top \tag{2}$$

$$\text{Attention: } S = \psi_{\delta_Q \delta_K}^{-1}(\hat{Q} \hat{K}^\top) + \Delta S, \quad (m', \tilde{P}) = \tilde{\sigma}(m, S), \quad (\delta_P, \hat{P}) = \psi_P(\tilde{P})$$

$$O = \text{diag}(\exp(m' - m)) O + \psi_{\delta_P \delta_V}^{-1}(\hat{P} \hat{V}) \tag{3}$$

$\phi_Q, \phi_K, \phi_V$  are three transformations to obtain quantized  $Q, K,$  and  $V$ , which we will discuss in subsequent sections. For simplicity, we omit all superscripts and subscripts, but the matrices used in attention are still tiles, and the computation is still organized as FlashAttention described in Section 2.1. Compared to the original full-precision version, as shown in Eq. 2, 3, `SageAttention2` adds quantizers to  $Q, K, P, V$  and dequantizers to the product to accelerate both Matmuls of  $QK$  and  $\tilde{P}V$ .

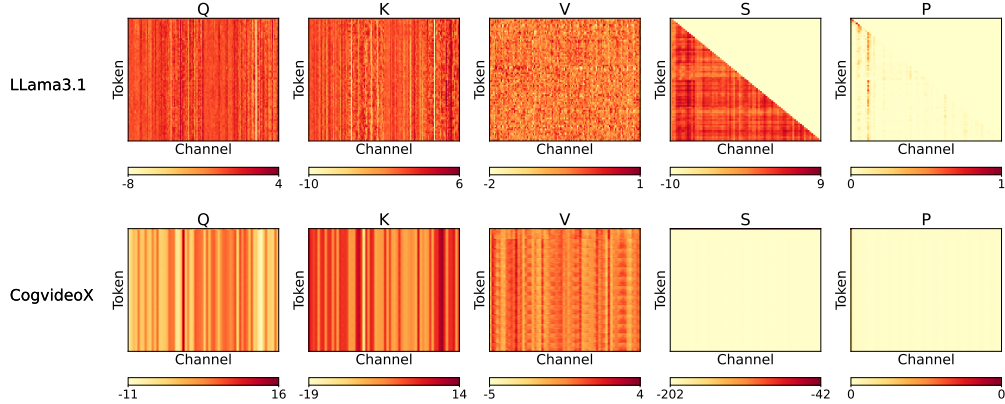


Figure 4: Typical examples of tensors’ data distribution in attention.

Table 1: End-to-end metrics comparison of different quantization methods, where Q,K are quantized into INT4, while P,V stay in full precision.

Q, K	Smoothing (Q+K)	Llama3.1 (Lambda) $\uparrow$	Llama3.1 (WikeText) $\downarrow$	CogVideo (vqa-a) $\uparrow$	CogVideo (vqa-t) $\uparrow$
Full-Precision	-	81.5%	6.013	77.605	75.360
INT4 Quantization	$\times$	72.6%	11.698	27.114	24.670
	$\checkmark$	80.8%	6.219	77.276	75.147

### 3.2 Per-warp INT4 Quantization

SageAttention uses per-block quantization, which quantizes each block of  $Q$  and  $K$  for a GPU streaming processor. Such a quantization strategy could achieve an accuracy performance close to per-token quantization and avoid the overhead of the dot product of the quantization scale vectors  $\delta_Q$  and  $\delta_K$ . However, quantizing  $Q$  and  $K$  to INT4 demands a more accurate quantization granularity. We propose *per-warp quantization*,

Table 2: **Average accuracy** across all layers using different quantization granularities.

Method	Cos Sim $\uparrow$	Relative L1 $\downarrow$	RMSE $\downarrow$
Per-token	99.45%	0.0649	0.0335
Per-warp	<b>99.45%</b>	<b>0.0648</b>	<b>0.0334</b>
Per-block	98.03%	0.1492	0.0744
Per-tensor	97.15%	0.1800	0.0865

Table 3: **Worst accuracy** across all layers using different quantization granularities.

Method	Cos Sim $\uparrow$	Relative L1 $\downarrow$	RMSE $\downarrow$
Per-token	96.76%	0.1916	0.0775
Per-warp	<b>96.71%</b>	<b>0.1956</b>	<b>0.0779</b>
Per-block	90.68%	0.3615	0.1490
Per-tensor	85.85%	0.4687	0.2261

a more precise and granular quantization approach than the *per-block quantizer*, also with no additional overhead of vectors dot product.

Specifically, each block of  $Q$  in SageAttention will be split into  $c_w$  segments, each processed by one of  $c_w$  GPU warps in a GPU streaming processor (SM). Subsequently, each warp performs Matmul for its assigned segment. Per-warp INT4 quantization assigns a scale factor for every  $b_q/wc$  tokens for  $Q$ :

$$\hat{Q}\left[\frac{i * b_q}{c_w} : \frac{b_q * (i + 1)}{c_w}, : \right] = \left[ \frac{Q\left[\frac{i * b_q}{c_w} : \frac{b_q * (i + 1)}{c_w}, : \right]}{\delta_Q[i]} \right] \quad (4)$$

$$\delta_Q[i] = \frac{\max\left(\left| Q\left[\frac{i * b_q}{c_w} : \frac{b_q * (i + 1)}{c_w}, : \right] \right|\right)}{7} \quad (5)$$

Per-warp quantization will provide an accuracy performance superior to per-block quantization used in SageAttention, which we will discuss in Section 3.5.

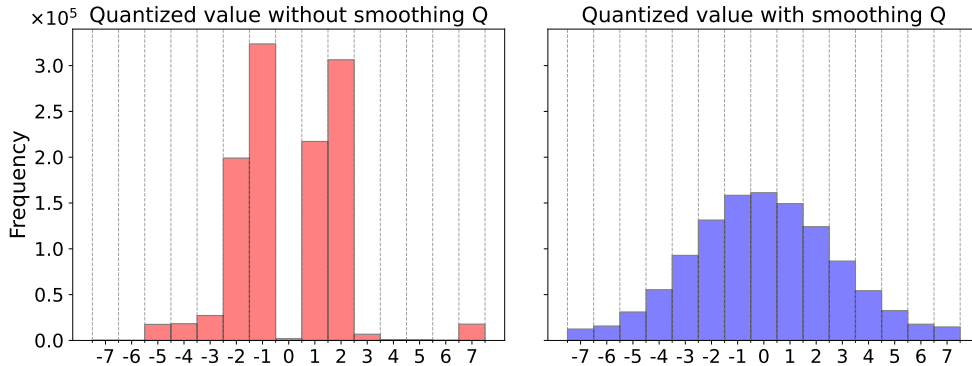


Figure 5: An example of quantized value distribution of  $Q$  before and after smoothing  $Q$ .

### 3.3 Smooth Q

The representative range for quantization of INT4 is notably restrictive, i.e., only  $2^4 - 1 = 15$  values. This limitation significantly degrades performance when quantizing  $Q, K$  into INT4 in attention. For example, using INT4 to quantize  $Q, K$  can cause the perplexity of Llama3.1 on WikiText to increase by more than 90%, and the quality of videos generated by CogvideoX decrease about 3x (See Table 1). We analyze the data distribution of  $Q, K$  in real models. For example, we find that Llama3.1 and CogvideoX show distinct channel-wised outliers in  $Q, K$  (See Figure 4). While per-channel quantization could mitigate the

quantization error caused by such outliers, this method is impracticable for  $Q, K$  because quantization must be conducted along the outer axis (token dimension) of  $QK^\top$ .

To address this challenge, we propose a method to eliminate the quantization error brought by the outliers in  $Q, K$ :

$$\begin{aligned}\overrightarrow{Q}_m &= \text{mean}(Q), \quad \gamma(Q) = Q - \overrightarrow{Q}_m, \quad \gamma(K) = K - \text{mean}(K), \\ S &= QK = \gamma(Q)\gamma(K) + \overrightarrow{Q}_m\gamma(K) \\ \phi_Q(Q) &= \psi_Q \circ \gamma(Q), \quad \overrightarrow{Q}_m, \quad \phi_K(K) = \psi_K \circ \gamma(K)\end{aligned}\tag{6}$$

Where  $\text{mean}(K)$  and  $\gamma(K)$  have been discussed in SageAttention (Zhang et al., 2024), and the transformation for  $K$  does not change the attention score  $\tilde{P}$ .  $\text{mean}(Q) = \frac{1}{N} \sum_{t=1}^N Q[t, :]$  is a vector with a shape  $1 \times d$ . For the transformation of  $Q$ , we will perform a GEMV (general matrix-vector multiplication) between  $\overrightarrow{Q}_m$  and  $K^\top$ , i.e.,  $\overrightarrow{Q}_m K^\top$  as  $\Delta S$ . This  $\Delta S$  will be added to  $S$  during the attention computation. Finally, the transformation from full-precision  $Q, K$  to quantized  $\hat{Q}, \hat{K}$  can be expressed as shown in Equation 6, where  $\psi_Q, \psi_K$  is two quantizers for  $Q$  and  $K$ . In other words, full-precision  $Q, K$  are subtracted with the means of the channel dimension before being quantized.

Figure 5 shows an example from CogvideoX of the distribution of quantized  $Q$  with and without smoothing  $Q$ . We can find that with smoothing  $Q$ , the range of INT4 is utilized more uniformly and fully. Table 1 presents end-to-end metrics for different quantization methods with and without *smoothing*  $Q+K$  on Llama3.1 (Dubey et al., 2024) and CogvideoX (Yang et al., 2024). The results demonstrate that *smoothing*  $Q+K$  offers significant accuracy benefits. Also, Table 9 and Table 10 show that the order of effectiveness is *smoothing*  $Q+K > \text{smoothing } Q > \text{smoothing } K > \text{other baselines}$ .

---

**Algorithm 1** Implementation of SageAttention2.

---

**Input:** Matrices  $Q(\text{FP16}), K(\text{FP16}), V(\text{FP16}) \in \mathbb{R}^{N \times d}$ , block size  $b_q, b_{kv}$ , warp count  $c_w$ .

**Preprocessing:**  $K = K - \text{mean}(K)$ ,  $\overrightarrow{Q}_m = \text{mean}(Q)$ ,  $Q = Q - \overrightarrow{Q}_m$ ,  $\Delta S = \text{GEMV}(\overrightarrow{Q}_m, K^\top)$ ,  $\overrightarrow{V}_m = \text{mean}(V)$ ,  $V = V - \overrightarrow{V}_m$ .

**Quantization:**  $(\delta_Q, \hat{Q}) = \psi_Q(Q)$  // INT4 Per-warp.  $(\delta_K, \hat{K}) = \psi_K(K)$ .  $(\delta_V, \hat{V}) = \psi_V(V)$ . // FP8 Per-channel.

Divide  $\hat{Q}$  to  $T_m = N/b_q$  blocks  $\{\hat{Q}_i\}$ ; divide  $\hat{K}, \hat{V}$ , and  $\Delta S$  to  $T_n = N/b_{kv}$  blocks  $\{\hat{K}_i\}, \{\hat{V}_i\}$ , and  $\{\Delta S_i\}$ ;  
**for**  $i = 1$  **to**  $T_m$  **do**

Load  $\hat{Q}_i$  and  $\delta_Q[i * c_w : (i + 1) * c_w]$  into an SM ;

**for**  $j$  in  $[1, T_n]$  **do**

Load  $\hat{K}_j, \hat{V}_j$ , and  $\delta_K[j]$  into the SM ;

$w = \text{range}(c_w), st = w * c_w$

$S_i^j[st : st + c_w] = \text{Matmul}(\hat{Q}_i[st : st + c_w], \hat{K}_j^\top) \times \delta_Q[st + w] \times \delta_K[j] + \Delta S_j$ ; // Paralleled by  $c_w$  warps.

$m_i^j = \max(m_i^{j-1}, \text{rowmax}(S_i^j))$ ,  $\tilde{P}_i^j = \exp(S_i^j - m_i^j)$ ,  $l_i^j = e^{m_i^{j-1} - m_i^j} + \text{rowsum}(\tilde{P}_i^j)$  ;

$O_i^j = \text{diag}(e^{m_i^{j-1} - m_i^j})^{-1} O_i^{j-1} + \text{Matmul}((\tilde{P}_i^j * 448).to(\text{FP8.e4m3}), V_j)$  ;

**end for**

Load  $\delta_V$  into an SM;

$O_i = \text{diag}(l_i^{T_n})^{-1} O_i^{T_n} / 448 * \delta_V$  ;

Write  $O_i$  ;

**end for**

$O = \{O_i\}$ ,  $O = O + \overrightarrow{V}_m$ .

**return**  $O$

---

Table 4: **Average accuracy** using different data types of  $(\tilde{P}, V)$  across all layers of a CogvideoX model, where  $(Q, K)$  are smoothed.

$Q, K$	$\tilde{P}, V$	Cos Sim $\uparrow$	Relative L1 $\downarrow$	RMSE $\downarrow$
INT4	INT8	77.05%	0.5618	0.5044
	E5M2	99.20%	0.0905	0.0903
	<b>E4M3</b>	<b>99.44%</b>	<b>0.0683</b>	<b>0.0347</b>
	FP16	99.45%	0.0649	0.0335

Table 5: **Worst accuracy** using different data types of  $(\tilde{P}, V)$  across all layers of a CogvideoX model, where  $(Q, K)$  are smoothed.

$Q, K$	$\tilde{P}, V$	Cos Sim $\uparrow$	Relative L1 $\downarrow$	RMSE $\downarrow$
INT4	INT8	19.52%	0.9579	1.4483
	E5M2	94.94%	0.2327	0.2361
	<b>E4M3</b>	<b>96.70%</b>	<b>0.1956</b>	<b>0.0779</b>
	FP16	96.76%	0.1916	0.0775

Table 6: An accuracy example on real tensors of CogvideoX model with or without smoothing  $V$ .

Smooth $V$	Cos Sim $\uparrow$	Relative L1 $\downarrow$	RMSE $\downarrow$
$\times$	98.25%	0.1980	0.2387
$\checkmark$	<b>99.75%</b>	<b>0.0406</b>	<b>0.0773</b>

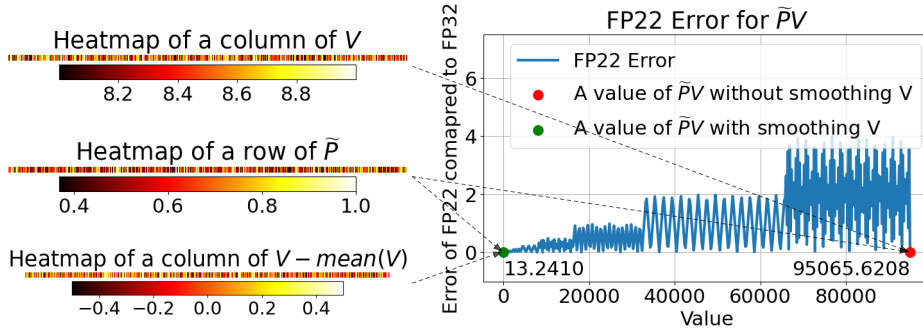


Figure 6: An example of dot product precision a row of  $\tilde{P}$  and a column of  $V$  presented by FP22 data type.

Table 7: Error of the FP8 Matmul instruction of  $mma(f8f8f32)$ .

Precision of Accumulated Value	E8M13	E8M23
Error compared to FP32	0	$ mma(f32.f16.f16.f32) - mma(f32.f8.f8.f32) $

### 3.4 Smooth $V$

To avoid the drawback of SageAttention where FP16 Matmul with an FP16 accumulator for  $PV$  is only effective on GPUs such as the RTX4090, we adopt the approach of quantizing  $P$  and  $V$  to FP8 to leverage the universal acceleration of FP8 Tensor cores. However, we discover that the accumulator for the  $mma(f32f8f8f32)$  instruction on the Ada architecture is actually FP22, specifically with 1 sign bit, 8 exponent bits, and 13 mantissa bits. Specifically, for  $mma(f32f8f8f32)$  instruction  $C = AB + D$ , where  $A, B$  are tensors in FP8 data type and  $C, D$  are tensors with FP32 data type, we initialize the  $A, B$  to zero and vary  $D$  to test the data type of the accumulator. As shown in Table 7, when  $D$  is initialized with 1 sign bit, 8 exponent bits, and 13 mantissa bits, the value of  $C$  matches the result of the  $mma(f16f16f32)$  instruction. However, when  $D$  is initialized with more than 13 mantissa bits, the error of  $C$  corresponds to the difference between the results of  $mma(f32f16f16f32)$  and  $mma(f32f8f8f32)$ . Consequently, matrix multiplication of matrices  $\tilde{P}$  and  $V$ , quantized to FP8, incurs a certain degree of precision loss compared to using an FP32 accumulator. To mitigate this precision loss as much as possible, we propose to smooth  $V$ :

$$\begin{aligned}\gamma(V) &= V - \text{mean}(V), \quad \text{mean}(V) = \vec{V}_m \\ \phi_V(V) &= \psi_V \circ \gamma, \quad \vec{V}_m\end{aligned}\tag{7}$$

As shown in Figure 6, this strategy enhances the accuracy of FP22 for values in  $\tilde{P}V$  for the following reasons: Each row of  $\tilde{P}$  spans a value range from 0 to 1, and each column of  $V$  consistently features channel-wise outliers that are exclusively positive or negative, typically ranging between 8 and 9. Consequently, the values of  $\tilde{P}V$  could be quite large. However, the floating-point number representation range is not uniform—it is denser near zero. Therefore, by subtracting the mean along the channel dimension from  $V$ , the values of  $\tilde{P}V$  will be closer to zero, resulting in higher representational precision. We believe such an explanation and strategy could address lots of issues<sup>1</sup> reported by the community. Additionally, to maintain the correctness of the attention computation, it is only necessary to add  $\vec{V}_m$  to the final calculation of  $O$ :  $O = O + \vec{V}_m$ . This is because the sum of each row of the  $\tilde{P}$  matrix equals 1, so  $\tilde{P}\vec{V}_m = \vec{V}_m$ . In other words, this method decomposes  $V$  into two parts:  $\vec{V}_m$  and  $V$ . For  $V$ , it centers the values of each column around zero, which leads to the dot product result of a row from the quantized  $\tilde{P}$  matrix with a column from the quantized  $V$  matrix being closer to zero. This makes the representation of FP22 more accurate. Meanwhile,  $\vec{V}_m$  is retained in FP16 and added to  $O$  at the end without causing a loss of precision for the  $\vec{V}_m$  part.

Table 6 shows the attention accuracy on real tensors sampled from `CogvideoX` with and without smoothing  $V$ . It demonstrates that smoothing  $V$  could improve the accuracy of `SageAttention2` when quantizing  $Q, K$  to INT4 and  $\tilde{P}, V$  to FP8.

### 3.5 Quantization for $Q, K, P, V$

**Quantization for  $Q, K$ .** We propose  $\psi_Q(Q)$  and  $\psi_K(K)$  in granularity of per-warp. This is first because per-channel quantization is not feasible since the scale factors of the inner axis of  $QK^\top$  cannot be used to do dequantization (Xiao et al., 2023a). Second, as shown in Table 2 and Table 3, we compare the average and worst-case accuracies of INT4 quantization at per-token, per-warp, per-block, and per-tensor granularity using real  $Q, K, V$  across all layers of `CogvideoX`. Results indicate that the accuracy of per-warp quantization is very close to per-token and outperforms a lot than per-block and per-tensor. Furthermore, per-warp quantization incurs less dequantization overhead than per-token as discussed in Section 3.2.

**Quantization for  $\tilde{P}, V$ .** We choose FP8, specifically the E4M3 data type, for  $\psi_P(\tilde{P})$  and  $\psi_V(V)$  for two reasons. First, most GPUs have tensor cores that support FP8 Matmul operations, which are twice as fast as those using FP16. Second, Table 4 and Table 5 show the average and worst accuracy of different data types used for  $\tilde{P}, V$  using real  $Q, K, V$  across all layers of `CogvideoX`. We can see that the accuracy of using E4M3 is very close to that of using FP16 and superior to that of E5M2 and INT8. We propose to use  $\psi_P(\tilde{P})$  in per-block and  $\psi_V(V)$  in per-channel for three reasons. First, per-channel quantization for  $\tilde{P}$  and per-token quantization for  $V$  are not viable because dequantization requires scale factors of outer axis. Second,  $\tilde{P} = \exp(S_i - \text{rowmax}(S_i))$ , where  $S_i$  is the Matmul result of a block of  $Q$  and  $K^\top$ , the max value in each row of  $\tilde{P}$  is 1. Hence, we can assign a single static scale  $s = \frac{1}{448}$  to a block  $\tilde{P}$ , whose accuracy **equals per-token quantization**. Third, per-channel quantization can address the channel-wised outlier of  $V$ .

**Accuracy metrics.** We use three metrics to assess the accuracy of quantized attention output  $O'$  compared to attention output in full-precision  $O$ : First, we flatten  $O'$  and  $O$  into vectors in the shape of  $1 \times n$ . Then, Cosine similarity:  $\text{CosSim} = \sum OO' / \sqrt{\sum O^2} \sqrt{\sum O'^2}$ , Relative L1 distance:  $L1 = \sum |O - O'| / \sum |O|$ , Root mean square error:  $\text{RMSE} = \sqrt{(1/n) \sum (O - O')^2}$ .

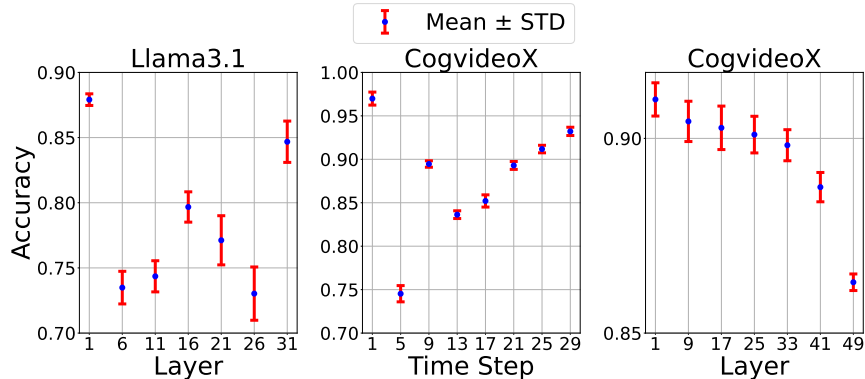
### 3.6 Adaptive Quantization over Layer and Timestep

Based on the discussion in Section 3.5, we implement two attention kernels (See Table 8) based on a choice: Using INT4 or INT8 quantization for  $\psi_Q(Q)$  and  $\psi_K(K)$ . The speed of these kernels is in the

<sup>1</sup><https://github.com/triton-lang/triton/issues/4476>, <https://github.com/triton-lang/triton/issues/5065>

Table 8: Two kernel implementations of SageAttention2.

Kernel	$\psi_Q(Q), \psi_K(K)$	$\psi_P(\tilde{P}), \psi_V(V)$
SageAttn2-4b	INT4, per-warp	FP8, per-block; FP8, per-channel
SageAttn2-8b	INT8, per-warp	FP8, per-block; FP8, per-channel

Figure 7: Mean and standard deviation of  $\text{cossim} * (1 - L1)$  of SageAttn-4b in different layers and timesteps for different inputs in Llama3.1 and CogvideoX.

order (SageAttn2-4b > SageAttn2-8b), but the accuracy order is opposite. Although SageAttn2-4b could perform adequately in lots of tasks, for instance, it shows very slight end-to-end metric loss of Lambda benchmark on Llama3.1, SageAttn2-4b falls short in some hard scenarios. Consequently, we first conduct a detailed analysis of the accuracy performance on various models using SageAttn2-4b and SageAttn2-8b. Then, we propose an effective and easy-to-use adaptive method.

**Accuracy across layers and timesteps.** Figure 7 displays the mean and standard deviation of the accuracy, calculated using  $\text{CosSim} * (1 - L1)$ , for SageAttn-4b across different layers and timesteps of different inputs in Llama3.1 and CogvideoX. It can be observed that specific layers and timesteps exhibit specific ranges of errors.

**Our method.** Our adaptive strategy is detailed as follows: First, we assess the average accuracy of SageAttn2-4b in comparison to full precision attention for each (layer, timestep) combination within a model, using several random inputs. For models without a timestep dimension, such as language models, the evaluation is confined to the layer dimension. Second, we will sort the (layer, timestep) combinations in descending order based on their  $\text{CosSim} * (1 - L1)$  values. We then identify the smallest  $\xi\%$  of these combinations. Finally, for the identified (layer, timestep) combinations, we consistently apply SageAttn2-8b across all other prompts. We call such a strategy SageAttn-mix and will report the values of  $\xi\%$  we used for each model in Section 4.1.

## 4 Experiment

### 4.1 Setup

**Models.** We validate the effectiveness of SageAttention2 across a diverse set of representative models from language, image, and video generation. Specifically, we conduct experiments on five models: Llama2 (7B) (Touvron et al., 2023), Llama3.1 (8B) (Dubey et al., 2024), and GLM4 (9B) (GLM et al., 2024) for text2text, CogvideoX (2B) (Yang et al., 2024) and Open-Sora (Zheng et al., 2024) for text2video, Flux (schnell) (Black Forest Labs, 2023) for text2image, and TIMM (Wightman, 2019) for image classification.

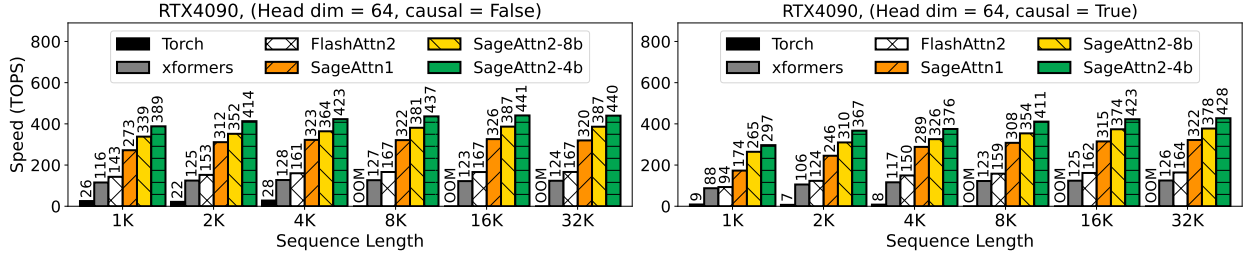


Figure 8: Speed comparison between SageAttention2 and baselines (RTX4090, headdim=64).

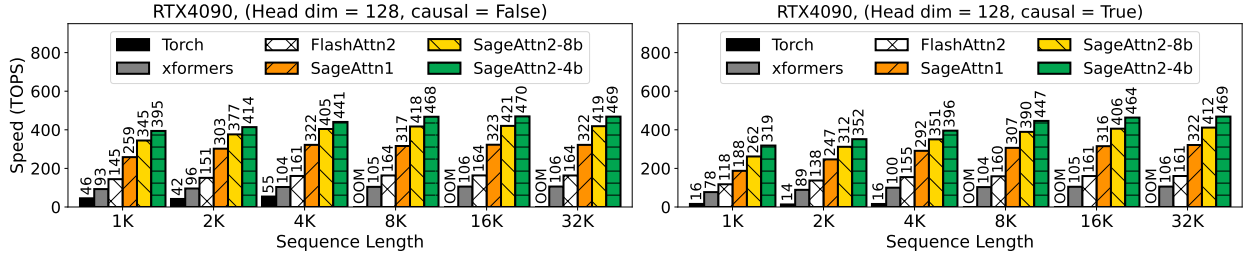


Figure 9: Speed comparison between SageAttention2 and baselines (RTX4090, headdim=128).

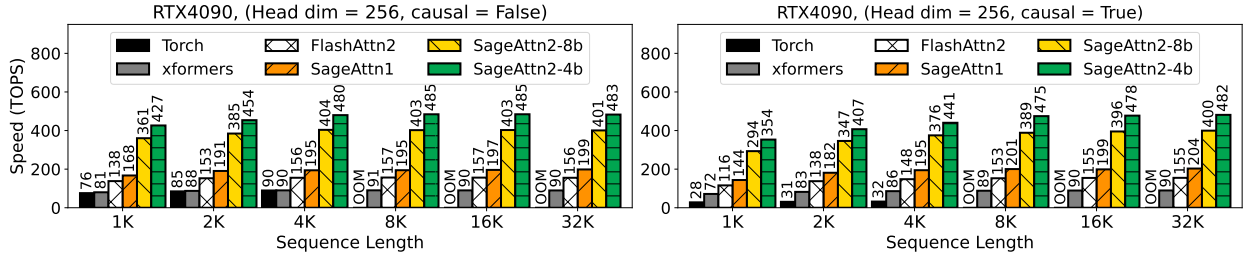


Figure 10: Speed comparison between SageAttention2 and baselines (RTX4090, headdim=256).

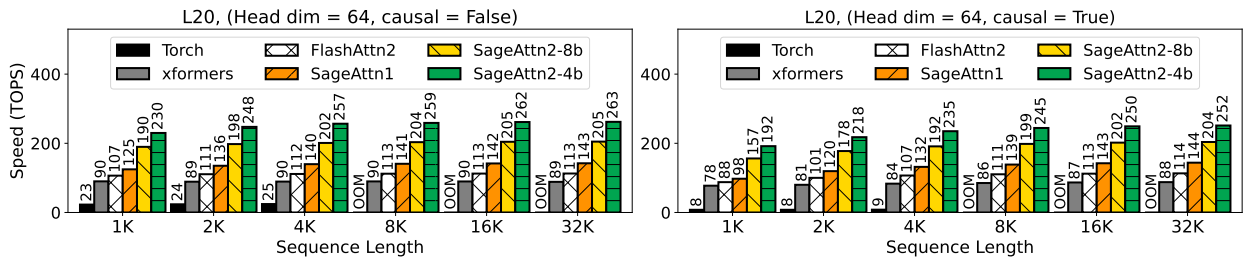


Figure 11: Speed comparison between SageAttention2 and baselines (L20, headdim=64).

**Datasets.** Text-to-text models are evaluated on four zero-shot tasks: WikiText (Merity et al., 2022) to assess the model’s prediction confidence, LAMBADA (Paperno et al., 2016) evaluate contextual understanding, MMLU (Hendrycks et al., 2020) for measuring knowledge across various subjects, and Longbench (Bai et al., 2023) for evaluating bilingual, multitask, and comprehensive assessment of long context understanding capabilities. Text-to-video models are evaluated using the open-sora (Zheng et al., 2024) prompt sets. Flux is



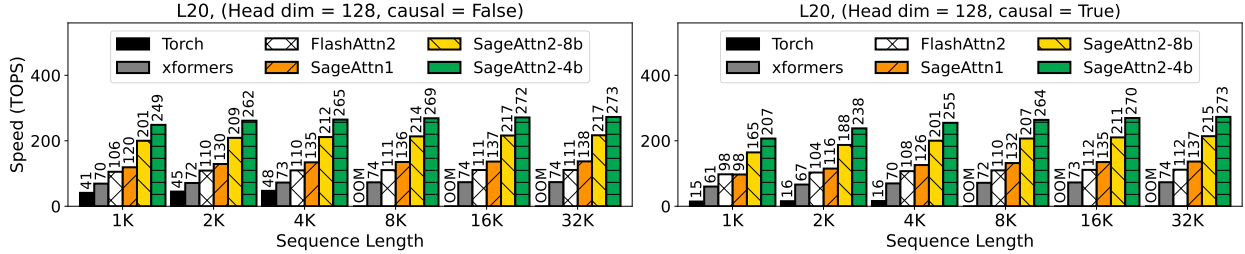


Figure 12: Speed comparison between SageAttention2 and baselines (L20, headdim=128).

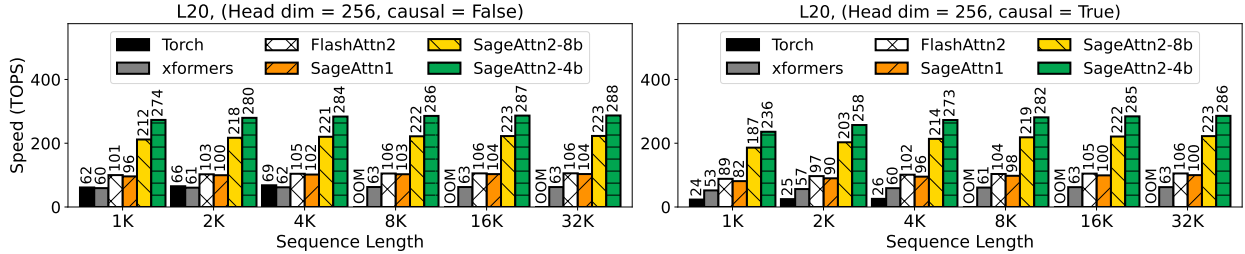


Figure 13: Speed comparison between SageAttention2 and baselines (L20, headdim=256).

assessed on MJHQ-30K (Li et al., 2024). TIMM is evaluated on on three image datasets: ImageNet (Deng et al., 2009), ImageNet-Sketch (Sketch) (Wang et al., 2019), and ImageNet-Rendition (ImageNet-r) (Hendrycks et al., 2021).

**Metrics.** For text-to-text models, we use perplexity (ppl.) (Jelinek et al., 1977) for WikiText, Accuracy (Acc.) for LAMBADA and MMLU, and Longbench score (Bai et al., 2023). For text-to-video models, following Zhao et al. (2024), we evaluate the quality of generated videos on five metrics: CLIPSIM and CLIP-Temp (CLIP-T) (Liu et al., 2024) to measure the text-video alignment; (VQA-a) and (VQA-t) to assess the video aesthetic and technical quality, respectively; and Flow-score (FScore) for temporal consistency (Wu et al., 2023). For text-to-image models, generated images are compared with the images in MJHQ-30K dataset in three aspects: FID (Heusel et al., 2017) and sFID (Salimans et al., 2016) for fidelity evaluation, *Clipscore* (CLIP) (Hessel et al., 2021) for text-image alignment, and *ImageReward* (IR) (Xu et al., 2024) for human preference. For TIMM, we use Accuracy.

**Implementation details.** We implement our attention kernels using CUDA and conduct experiments on Ubuntu 22.04 servers with RTX4090 and L20 GPUs.

**Baselines.** (1) *SmoothAttn*. Following Qserve (Lin et al., 2024), we apply smooth quant for matrixes  $Q, K$  with smoothing factor  $\alpha = 0.5$ . (2) *HadmdAttn*. Following Quarot (Ashkboos et al., 2024), we apply random Hadamard transformation for matrixes  $Q, K$  before INT4 quantization.

**Hyper-parameters of SageAttn-mix.** We use  $\xi$  of 50% for Llama2, 60% for CogvideoX, 25% for Open-Sora, 30% for Llama3.1 and GLM4, 0% for Flux, and TIMM.

## 4.2 Speed and Accuracy of Kernels

**Speed.** We conduct experiments to compare the Speed of SageAttention2 against baselines using configurations with headdim=64, headdim=128, and headdim=256, both with and without Causal Mask (Vaswani, 2017). Specifically, Figure 8, Figure 9, and Figure 10 show the speed of SageAttention2 and baselines across varying sequence lengths on RTX4090. These results indicate that SageAttention2 achieves a peak of 485 TOPS and is 3.1x faster than FlashAttention2 and 5.4x faster than xformers. Figure 11, Figure 12, and Figure 13 illustrate the results on L20 GPU, indicating that SageAttention2 achieves a peak of 288

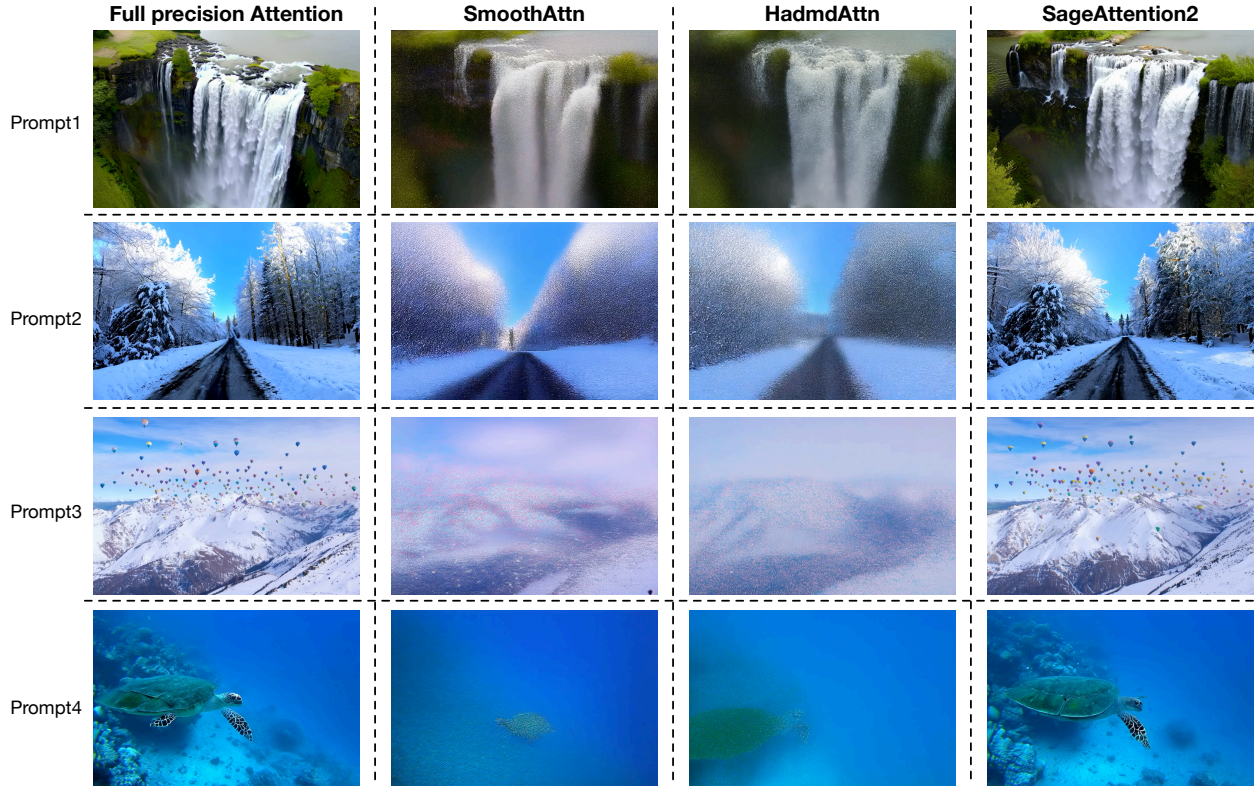


Figure 14: Comparison examples from CogvideoX, prompts are sampled from open-sora prompt sets.

Table 9: **Average accuracy** across all layers using different smooth methods.

Method	CosSim $\uparrow$	Relative L1 $\downarrow$	RMSE $\downarrow$
None	80.04%	0.3906	0.2223
HadmdAttn	79.77%	0.3782	0.2180
SmoothAttn	90.21%	0.3383	0.1952
Smooth K (Ours)	98.07%	0.1493	0.0743
Smooth Q (Ours)	98.30%	0.1250	0.0712
SageAttn2-4b	<b>99.46%</b>	<b>0.0648</b>	<b>0.0334</b>

Table 10: **Worst accuracy** across all layers using different smooth methods.

Method	CosSim $\uparrow$	Relative L1 $\downarrow$	RMSE $\downarrow$
None	4.83%	0.9979	0.7784
HadmdAttn	4.85%	0.9978	0.7785
SmoothAttn	64.49%	0.9262	0.7204
Smooth K (Ours)	90.86%	0.3565	0.1464
Smooth Q (Ours)	93.10%	0.2989	0.2195
SageAttn2-4b	<b>96.71%</b>	<b>0.1956</b>	<b>0.0779</b>

TOPS and is **2.7x** faster than FlashAttention2 and **4.6x** faster than xformers.

**Accuracy.** Table 9 and Table 10 show that the average and worst accuracy of different methods with INT4  $Q, K$  and FP8  $P, V$  across all layers of CogvideoX. The results indicate that the accuracy of SageAttn-4b is superior to other baselines.

### 4.3 End-to-end Performance

**Metrics loss.** We assessed the end-to-end metrics of various models using SageAttention2 compared to using attention in full precision. Detailed evaluation results are presented in Table 11 for Llama2, Llama3.1, GLM4, CogvideoX, Open-Sora, Flux, and TIMM, respectively. The results indicate that SageAttn-4b outperforms all baselines and maintains most of the end-to-end accuracy across all models. Additionally, using

Table 11: End-to-end metrics loss across text, image, and video generation models.

Model	Attention	WikiText (Ppl.) ↓	Lambda (Acc.) ↑	MMLU (Acc.) ↑	Longbench ↑
Llama2	Full-Precision	5.823	0.886	0.439	-
	HadmdAttn	6.706	0.865	0.355	-
	SmoothAttn	6.690	0.871	0.395	-
	<b>SageAttn2-4b</b>	<b>6.018</b>	<b>0.886</b>	<b>0.436</b>	-
	<b>SageAttn2-mix</b>	<b>5.883</b>	<b>0.883</b>	<b>0.431</b>	-
Llama3.1	Full-Precision	6.013	0.815	0.635	49.40
	HadmdAttn	7.661	0.756	0.502	44.62
	SmoothAttn	7.087	0.788	0.551	43.76
	<b>SageAttn2-4b</b>	<b>6.219</b>	<b>0.808</b>	<b>0.617</b>	<b>48.61</b>
	<b>SageAttn2-mix</b>	<b>6.131</b>	<b>0.816</b>	<b>0.629</b>	<b>49.01</b>
GLM4	Full-Precision	7.241	0.432	0.743	49.78
	HadmdAttn	7.932	0.435	0.676	46.27
	SmoothAttn	8.841	0.442	0.599	43.10
	<b>SageAttn2-4b</b>	<b>7.341</b>	<b>0.435</b>	<b>0.732</b>	<b>49.06</b>
	<b>SageAttn2-mix</b>	<b>7.303</b>	<b>0.434</b>	<b>0.737</b>	<b>49.77</b>

Model	Attention	CLIPSIM ↑	CLIP-T ↑	VQA-a ↑	VQA-t ↑	FScore ↑
CogvideoX	Full-Precision	0.1836	0.9975	77.605	75.360	3.006
	HadmdAttn	0.1742	0.9877	36.028	23.786	0.550
	SmoothAttn	0.1763	0.9870	37.444	42.184	0.792
	<b>SageAttn2-4b</b>	<b>0.1813</b>	<b>0.9969</b>	<b>77.276</b>	<b>75.147</b>	<b>2.070</b>
	<b>SageAttn2-mix</b>	<b>0.1816</b>	<b>0.9976</b>	<b>75.686</b>	<b>78.600</b>	<b>2.884</b>
Open-Sora	Full-Precision	0.1831	0.9996	46.713	59.553	0.368
	<b>SageAttn2-4b</b>	<b>0.1821</b>	<b>0.9994</b>	<b>42.270</b>	<b>55.965</b>	<b>0.364</b>
	<b>SageAttn2-mix</b>	<b>0.1814</b>	<b>0.9994</b>	<b>44.509</b>	<b>59.097</b>	<b>0.383</b>

Model	Attention	FID ↓	sFID ↓	CLIP ↑	IR ↑
Flux	Full-Precision	11.303	17.603	32.603	0.9745
	HadmdAttn	11.163	17.693	32.592	0.9638
	SmoothAttn	10.941	18.098	32.582	0.9613
	<b>SageAttn2-4b</b>	<b>10.563</b>	<b>17.052</b>	<b>32.631</b>	<b>0.9747</b>

Model	Attention	ImageNet (Acc.) ↑	Sketch (Acc.) ↑	ImageNet-r (Acc.) ↑
TIMM	Full-Precision	84.79%	45.32%	59.55%
	<b>SageAttn2-4b</b>	<b>84.67%</b>	<b>45.07%</b>	<b>59.11%</b>

adaptive quantization techniques, SageAttn-mix achieves performance comparable to full-precision attention.

#### 4.4 Ablation Study

**Adaptive quaitzation.** To analyze the impact of using different ratio of SageAttn-8b in adaptive quantization, Table 15 shows the changes in the perplexity of Llama3.1 under various ratio of SageAttn-8b. It can be observed that even if SageAttn-4b is used exclusively, the overall end-to-end representation is sufficiently good, and the higher the ratio of SageAttn-8b used, the closer the accuracy approaches that of using full-precision attention.

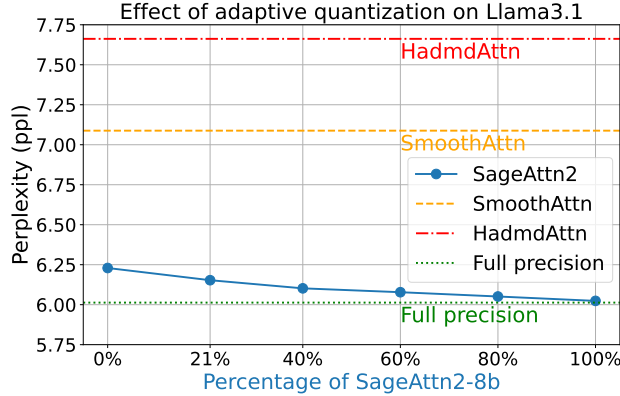


Figure 15: End-to-end performance using different ratio of SageAttn-8b.

**Overhead of smoothing  $Q, K$ .** Note that the overhead of smoothing  $Q, K$  only contains  $Q - \overrightarrow{Q}_m$ ,  $K - \text{mean}(K)$ , and  $\overrightarrow{Q}_m K^\top$ . The speed overhead of them accounts for about 3.5% of the attention kernel.

## 5 Conclusion and Future Work

We introduce **SageAttention2**, an efficient and accurate 4-bit quantization method for attention. First, we propose to quantize  $(Q, K)$  to INT4 in a warp-level granularity and quantize  $(\tilde{P}, V)$  to FP8. Second, we propose a method to smooth matrixes  $Q$  and  $V$ , enhancing the accuracy of attention with INT4  $QK$  and FP8  $PV$ . Third, we analyze the quantization accuracy across timesteps and layers, then propose an adaptive quantization method to ensure the end-to-end metrics over various models. Our implementation is faster than FlashAttention2 and xformers by approximately **3.1x** and **5.4x** on RTX4090, respectively. Extensive testing confirms that our approach maintains end-to-end metrics across various models, including language, image, and video generation.

**Future Work.** We leave the implementation of FP8 MatMul with an FP16 accumulator for  $\tilde{P}V$  and SageAttention2 on the Hopper architecture for future work.

## References

- Ashkboos, S., Mohtashami, A., Croci, M. L., Li, B., Cameron, P., Jaggi, M., Alistarh, D., Hoefler, T., and Hensman, J. Quarat: Outlier-free 4-bit inference in rotated llms, 2024. URL <https://arxiv.org/abs/2404.00456>.
- Bai, Y., Lv, X., Zhang, J., Lyu, H., Tang, J., Huang, Z., Du, Z., Liu, X., Zeng, A., Hou, L., et al. Longbench: A bilingual, multitask benchmark for long context understanding. *arXiv preprint arXiv:2308.14508*, 2023.
- Black Forest Labs. Flux. <https://github.com/black-forest-labs/flux>, 2023.
- Chen, Y., Qian, S., Tang, H., Lai, X., Liu, Z., Han, S., and Jia, J. Longlora: Efficient fine-tuning of long-context large language models. *arXiv preprint arXiv:2309.12307*, 2023.
- Choromanski, K., Likhoshesterov, V., Dohan, D., Song, X., Gane, A., Sarlos, T., Hawkins, P., Davis, J., Mohiuddin, A., Kaiser, L., et al. Rethinking attention with performers. *arXiv preprint arXiv:2009.14794*, 2020.

- Chu, X., Tian, Z., Wang, Y., Zhang, B., Ren, H., Wei, X., Xia, H., and Shen, C. Twins: Revisiting the design of spatial attention in vision transformers. *Advances in neural information processing systems*, 34: 9355–9366, 2021.
- Dao, T. Flashattention-2: Faster attention with better parallelism and work partitioning. *arXiv preprint arXiv:2307.08691*, 2023.
- Dao, T., Fu, D., Ermon, S., Rudra, A., and Ré, C. Flashattention: Fast and memory-efficient exact attention with io-awareness. *Advances in Neural Information Processing Systems*, 35:16344–16359, 2022.
- Deng, J., Dong, W., Socher, R., Li, L.-J., Li, K., and Fei-Fei, L. Imagenet: A large-scale hierarchical image database. In *2009 IEEE conference on computer vision and pattern recognition*, pp. 248–255. Ieee, 2009.
- Dubey, A., Jauhri, A., Pandey, A., Kadian, A., Al-Dahle, A., Letman, A., Mathur, A., Schelten, A., Yang, A., Fan, A., et al. The llama 3 herd of models. *arXiv preprint arXiv:2407.21783*, 2024.
- Fu, T., Huang, H., Ning, X., Zhang, G., Chen, B., Wu, T., Wang, H., Huang, Z., Li, S., Yan, S., Dai, G., Yang, H., and Wang, Y. Moa: Mixture of sparse attention for automatic large language model compression, 2024. URL <https://arxiv.org/abs/2406.14909>.
- Gao, Y., Zeng, Z., Du, D., Cao, S., So, H. K.-H., Cao, T., Yang, F., and Yang, M. Seerattention: Learning intrinsic sparse attention in your llms, 2024. URL <https://arxiv.org/abs/2410.13276>.
- gkamradt. Llmtest needle in a haystack - pressure testing llms. [https://github.com/gkamradt/LLMTest\\_NeedleInAHaystack](https://github.com/gkamradt/LLMTest_NeedleInAHaystack), 2023.
- GLM, T., Zeng, A., Xu, B., Wang, B., Zhang, C., Yin, D., Rojas, D., Feng, G., Zhao, H., Lai, H., Yu, H., Wang, H., Sun, J., Zhang, J., Cheng, J., Gui, J., Tang, J., Zhang, J., Li, J., Zhao, L., Wu, L., Zhong, L., Liu, M., Huang, M., Zhang, P., Zheng, Q., Lu, R., Duan, S., Zhang, S., Cao, S., Yang, S., Tam, W. L., Zhao, W., Liu, X., Xia, X., Zhang, X., Gu, X., Lv, X., Liu, X., Liu, X., Yang, X., Song, X., Zhang, X., An, Y., Xu, Y., Niu, Y., Yang, Y., Li, Y., Bai, Y., Dong, Y., Qi, Z., Wang, Z., Yang, Z., Du, Z., Hou, Z., and Wang, Z. Chatglm: A family of large language models from glm-130b to glm-4 all tools, 2024.
- Hendrycks, D., Burns, C., Basart, S., Zou, A., Mazeika, M., Song, D., and Steinhardt, J. Measuring massive multitask language understanding. 2020.
- Hendrycks, D., Basart, S., Mu, N., Kadavath, S., Wang, F., Dorundo, E., Desai, R., Zhu, T., Parajuli, S., Guo, M., Song, D., Steinhardt, J., and Gilmer, J. The many faces of robustness: A critical analysis of out-of-distribution generalization. *ICCV*, 2021.
- Hessel, J., Holtzman, A., Forbes, M., Le Bras, R., and Choi, Y. Clipscore: A reference-free evaluation metric for image captioning. In *Proceedings of the 2021 Conference on Empirical Methods in Natural Language Processing*, pp. 7514–7528, 2021.
- Heusel, M., Ramsauer, H., Unterthiner, T., Nessler, B., and Hochreiter, S. Gans trained by a two time-scale update rule converge to a local nash equilibrium. *Advances in neural information processing systems*, 30, 2017.
- Jelinek, F., Mercer, R. L., Bahl, L. R., and Baker, J. K. Perplexity—a measure of the difficulty of speech recognition tasks. *The Journal of the Acoustical Society of America*, 62(S1):S63–S63, 1977.
- Jiang, H., Li, Y., Zhang, C., Wu, Q., Luo, X., Ahn, S., Han, Z., Abdi, A. H., Li, D., Lin, C.-Y., et al. Minference 1.0: Accelerating pre-filling for long-context llms via dynamic sparse attention. *arXiv preprint arXiv:2407.02490*, 2024.
- Katharopoulos, A., Vyas, A., Pappas, N., and Fleuret, F. Transformers are rnns: Fast autoregressive transformers with linear attention. In *International conference on machine learning*, pp. 5156–5165. PMLR, 2020.

- Lefaudeux, B., Massa, F., Liskovich, D., Xiong, W., Caggiano, V., Naren, S., Xu, M., Hu, J., Tintore, M., Zhang, S., Labatut, P., Haziza, D., Wehrstedt, L., Reizenstein, J., and Sizov, G. xformers: A modular and hackable transformer modelling library. <https://github.com/facebookresearch/xformers>, 2022.
- Li, D., Kamko, A., Akhgari, E., Sabet, A., Xu, L., and Doshi, S. Playground v2.5: Three insights towards enhancing aesthetic quality in text-to-image generation, 2024.
- Li, K., Wang, Y., Peng, G., Song, G., Liu, Y., Li, H., and Qiao, Y. Uniformer: Unified transformer for efficient spatial-temporal representation learning. In *International Conference on Learning Representations*.
- Lin, Y., Tang, H., Yang, S., Zhang, Z., Xiao, G., Gan, C., and Han, S. Qserve: W4a8kv4 quantization and system co-design for efficient llm serving, 2024. URL <https://arxiv.org/abs/2405.04532>.
- Liu, Y., Cun, X., Liu, X., Wang, X., Zhang, Y., Chen, H., Liu, Y., Zeng, T., Chan, R., and Shan, Y. Evalcrafter: Benchmarking and evaluating large video generation models. In *Proceedings of the IEEE/CVF Conference on Computer Vision and Pattern Recognition*, pp. 22139–22149, 2024.
- Liu, Z., Lin, Y., Cao, Y., Hu, H., Wei, Y., Zhang, Z., Lin, S., and Guo, B. Swin transformer: Hierarchical vision transformer using shifted windows. In *Proceedings of the IEEE/CVF international conference on computer vision*, pp. 10012–10022, 2021.
- Merity, S., Xiong, C., Bradbury, J., and Socher, R. Pointer sentinel mixture models. In *International Conference on Learning Representations*, 2022.
- Milakov, M. and Gimelshein, N. Online normalizer calculation for softmax. *arXiv preprint arXiv:1805.02867*, 2018.
- Paperno, D., Kruszewski, G., Lazaridou, A., Pham, N.-Q., Bernardi, R., Pezzelle, S., Baroni, M., Boleda, G., and Fernández, R. The lambada dataset: Word prediction requiring a broad discourse context. In *Proceedings of the 54th Annual Meeting of the Association for Computational Linguistics (Volume 1: Long Papers)*, pp. 1525–1534, 2016.
- Salimans, T., Goodfellow, I., Zaremba, W., Cheung, V., Radford, A., and Chen, X. Improved techniques for training gans. *Advances in neural information processing systems*, 29, 2016.
- Shah, J., Bikshandi, G., Zhang, Y., Thakkar, V., Ramani, P., and Dao, T. Flashattention-3: Fast and accurate attention with asynchrony and low-precision. *arXiv preprint arXiv:2407.08608*, 2024.
- Touvron, H., Martin, L., Stone, K., Albert, P., Almahairi, A., Babaei, Y., Bashlykov, N., Batra, S., Bhargava, P., Bhosale, S., et al. Llama 2: Open foundation and fine-tuned chat models. *arXiv preprint arXiv:2307.09288*, 2023.
- Vaswani, A. Attention is all you need. *Advances in Neural Information Processing Systems*, 2017.
- Venkataramanan, S., Ghodrati, A., Asano, Y. M., Porikli, F., and Habibian, A. Skip-attention: Improving vision transformers by paying less attention. *arXiv preprint arXiv:2301.02240*, 2023.
- Wang, H., Ge, S., Lipton, Z., and Xing, E. P. Learning robust global representations by penalizing local predictive power. *Advances in Neural Information Processing Systems*, 32, 2019.
- Wang, S., Li, B. Z., Khabsa, M., Fang, H., and Ma, H. Linformer: Self-attention with linear complexity. *arXiv preprint arXiv:2006.04768*, 2020.
- Wightman, R. Pytorch image models. <https://github.com/rwightman/pytorch-image-models>, 2019.
- Wu, H., Zhang, E., Liao, L., Chen, C., Hou, J., Wang, A., Sun, W., Yan, Q., and Lin, W. Exploring video quality assessment on user generated contents from aesthetic and technical perspectives. In *Proceedings of the IEEE/CVF International Conference on Computer Vision*, pp. 20144–20154, 2023.

- Xiao, C., Zhang, P., Han, X., Xiao, G., Lin, Y., Zhang, Z., Liu, Z., and Sun, M. Infilmm: Training-free long-context extrapolation for llms with an efficient context memory. In *First Workshop on Long-Context Foundation Models@ ICML 2024*, 2024.
- Xiao, G., Lin, J., Seznec, M., Wu, H., Demouth, J., and Han, S. Smoothquant: Accurate and efficient post-training quantization for large language models. In *International Conference on Machine Learning*, pp. 38087–38099. PMLR, 2023a.
- Xiao, G., Tian, Y., Chen, B., Han, S., and Lewis, M. Efficient streaming language models with attention sinks. *arXiv preprint arXiv:2309.17453*, 2023b.
- Xu, J., Liu, X., Wu, Y., Tong, Y., Li, Q., Ding, M., Tang, J., and Dong, Y. Imagereward: Learning and evaluating human preferences for text-to-image generation. *Advances in Neural Information Processing Systems*, 36, 2024.
- Yang, Z., Teng, J., Zheng, W., Ding, M., Huang, S., Xu, J., Yang, Y., Hong, W., Zhang, X., Feng, G., et al. Cogvideox: Text-to-video diffusion models with an expert transformer. *arXiv preprint arXiv:2408.06072*, 2024.
- Yu, W., Luo, M., Zhou, P., Si, C., Zhou, Y., Wang, X., Feng, J., and Yan, S. Metaformer is actually what you need for vision. In *Proceedings of the IEEE/CVF conference on computer vision and pattern recognition*, pp. 10819–10829, 2022.
- Zhang, J., wei, J., Zhang, P., Zhu, J., and Chen, J. Sageattention: Accurate 8-bit attention for plug-and-play inference acceleration, 2024. URL <https://arxiv.org/abs/2410.02367>.
- Zhao, T., Fang, T., Liu, E., Rui, W., Soedarmadji, W., Li, S., Lin, Z., Dai, G., Yan, S., Yang, H., Ning, X., and Wang, Y. Vidit-q: Efficient and accurate quantization of diffusion transformers for image and video generation, 2024.
- Zheng, Z., Peng, X., Yang, T., Shen, C., Li, S., Liu, H., Zhou, Y., Li, T., and You, Y. Open-sora: Democratizing efficient video production for all, March 2024. URL <https://github.com/hpcaitech/Open-Sora>.